ACS OMEGA

http://pubs.acs.org/journal/acsodf

Article

Dynamics of Droplet Coalescence on Hydrophobic Fibers in Oil: Morphology and Liquid Bridge Evolution

Bingbing Li,* Wei Tan, Guiyu Liu, and Mo Huang

Cite This: *ACS Omega* 2023, 8, 18019−18028

Read Online

ACCESS | Metrics & More | Article Recommendations

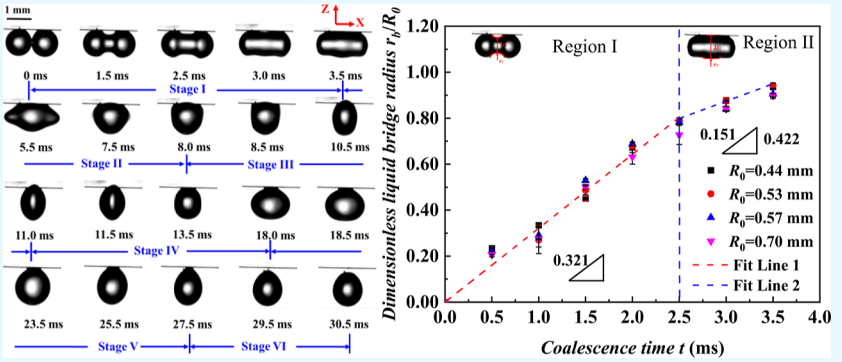

ABSTRACT: Although droplet self-jumping on hydrophobic fibers is a well-known phenomenon, the influence of viscous bulk fluids on this process is still not fully understood. In this work, two water droplets' coalescence on a single stainless-steel fiber in oil was investigated experimentally. Results showed that lowering the bulk fluid viscosity and increasing the oil−water interfacial tension promoted droplet deformation, reducing the coalescence time of each stage. While the total coalescence time was more influenced by the viscosity and under-oil contact angle than the bulk fluid density. For water droplets coalescing on hydrophobic fibers in oils, the expansion of the liquid bridge can be affected by the bulk fluid, but the expansion dynamics exhibited similar behavior. The drops begin their coalescence in an inertially limited viscous regime and transition to an inertia regime. Larger droplets did accelerate the expansion of the liquid bridge but had no obvious influence on the number of coalescence stages and coalescence time. This study can provide a more profound understanding of the mechanisms underlying the behavior of water droplet coalescence on hydrophobic surfaces in oil.

1. INTRODUCTION

Water pollution in oil is a common phenomenon in many industrial applications and can cause many problems, such as, water in jet fuel not only impacts the lubricative properties of fuel but also can freeze in sub-zero conditions restricting fuel flow and even can cause air crashes.[1,2] Hence, separating dispersion water from oil is necessary for safety, ecological, and economic reasons.[3,4]

Membrane separation techniques have been developed and considered as an effective technique for oil/water emulsion separation due to their environmental friendliness, cost-effectiveness, and high separation efficiency.[5,6] Nevertheless, pressure-driven oil/water separation membranes are often affected by fouling caused by heterogeneous particles deposited on the membrane surface, such as inorganic ions or salt deposits.[7,8] It can significantly reduce the performance of membrane separation and shorten the membrane lifetime. Effective methods for mitigating membrane fouling include regulating the mass transfer of the feed solution into the membrane modules, enhancing membrane cleaning procedures, and developing membranes with improved fouling resistance.[9] The techniques mentioned above have been utilized in many industries; however, these technologies suffer from high costs and complex operational steps.

Recently, coalescence-induced droplet jumping on hydrophobic surfaces has been shown to be a very effective way to achieve self-cleaning and anti-fouling without external forces.[10,11] As droplets coalesce, surface energy released during the coalescence process can drive the self-propelled jumping of the liquid droplets on superhydrophobic solid surfaces, and the jumping droplets can additionally carry particles toward self-cleaning.[12−17] This is an autonomous movement that clears liquid droplets without external forces, reducing solid particles'

Received: February 22, 2023
Accepted: May 3, 2023
Published: May 11, 2023

residence time and surface coverage, which may open new avenues for improving self-cleaning and anti-fouling of membranes for water−oil emulsion separation.

Droplet jumping behavior can be influenced not only by the microstructures of hydrophobic surfaces[18−25] and the characteristic of droplets[25−29] but also by the bulk fluids surrounding the droplets.[30−32] However, most of the work was limited to studying the behavior of water droplet coalescence and jumping in the air, and few mention the effects of bulk fluids on the droplet coalescence and jumping behavior. It has been reported that the properties of the bulk fluid can affect the merged behaviors of droplets. Farokhirad[31] used a multiphase lattice Boltzmann method to simulate the effects of air viscosity and density on the droplet bounce process. They found that increasing the viscosity of the air would inhibit the flow of the inner part of the liquid during droplet coalescence, while increasing the density of the air would increase the droplet's take-off height.

Furthermore, researchers have demonstrated that the dynamics of liquid bridge expansion of droplet coalescence also could be affected by bulk fluids.[33] At the early stages, the neck radius of the liquid bridge, $r(t)$, expands as a function of t, the time since initial contact, and the dynamics were determined by $r(t)/R_i \propto Oh$,[34−36] where Oh is the Ohnesorge number, which represents the ratio of internal viscosity dissipation to the surface tension energy, and R_i is the droplet radius. For droplet coalescence in air, the droplets usually begin their coalescence in the inertially limited viscous regime and then transition to the inertial regime[37−39] but for droplet coalescence in outer viscous fluids, the regime of droplet coalescence depends on the Ohnesorge number, which is related to the fluid properties of bulk fluids and droplets.[40,41]

In addition, unlike the droplet coalescence-induced jumping on superhydrophobic surfaces in air, in viscous bulk fluids, the effect of oil−water interfacial tension also needs to be considered in addition to the effect of viscosity and density of the bulk fluid.[42,43] All of these make the processes of droplet coalescence and jumping in viscous fluids more complicated. Therefore, complex events occurring in a viscous fluid are not adequately understood, and the influence of bulk fluids on droplet coalescence and jumping behaviors is crucial.

In this work, we are devoted to investigating the differences in the droplet coalescence and self-removal behavior on hydrophobic fibers in oils, and its potential applications in anti-fouling membranes for oil−water separation. We focused on identifying the differences in this behavior compared to previous studies in air-based systems. Our findings shed light on the potential of utilizing these properties for developing innovative anti-fouling strategies for oil−water separation membranes. *n*-Hexane (n-C_6H_{14}), *n*-dodecane (n-$C_{12}H_{26}$), and toluene (C_7H_8) were selected as the bulk fluids, and 304 stainless-steel fibers (SS) were chosen as a hydrophobic fiber under oil. The effects of bulk fluid viscosity, oil−water interfacial tension, under-oil water contact angle (WCA), and droplet size on the droplet coalescence and self-removal behaviors on the fibers were systematically studied to understand the dynamics of water droplet coalescence-induced jumping in viscous bulk fluids.

2. METHODS

2.1. Experimental Materials. In this paper, three different organic solvents (*n*-hexane (n-C_6H_{14}), *n*-dodecane (n-$C_{12}H_{26}$), and toluene (C_7H_8)) were chosen as bulk fluid. At room temperature, due to the similarity of oil-water interfacial tension between n-C_6H_{14} and n-$C_{12}H_{26}$, and the similarity of the viscosity between n-C_6H_{14} and C_7H_8, respectively, which is convenient to study the influence of bulk fluid properties on the dynamic behavior of water droplet coalescence-induced self-removal on the hydrophobic surface. All chemicals used here were purchased from Tianjin Yuanli Chemical Co., Ltd. (Tianjin, China). The physical properties of the bulk fluids are listed in Table 1. All the values were measured at 25 °C under atmospheric pressure.

Table 1. Various Liquid Parameters in the Experiments (25 °C)[a]

property	density ρ/g/cm^3	viscosity μ/mPa s	surface tension γ/mN/m	oil−water interfacial tension γ_{ow}/mN/m	under-oil WCA of 304 SS/°
n-C_6H_{14}	0.653	0.6393	17.52	50.51	115.50 ± 2
n-$C_{12}H_{26}$	0.740	1.3746	25.00	50.10	122.33 ± 1
C_7H_8	0.862	0.561	27.98	35.70	120.25 ± 2
deionized water	0.997	0.8937	71.97		

[a]All of the values are the average values of three individual measurements.

The under-oil hydrophobic fibers used here were 304 stainless-steel fibers (SS) with a radius of about 18 μm. Moreover, the fibers were thoroughly rinsed with deionized water, acetone, and alcohol and dried in air overnight before being used without additional treatment. Their WCA under-oil is listed in Table 1, and Figure 1 presents scanning electron microscopy (SEM) images of 304 SS fibers.

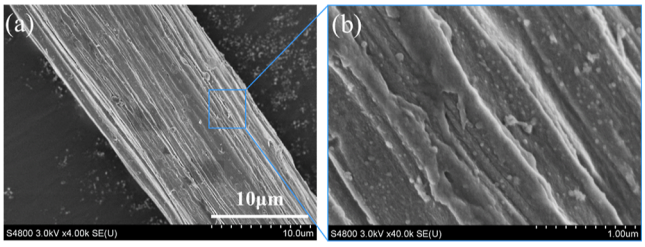

Figure 1. (a, b) SEM images of 304 stainless steel with a fiber radius of $r_f \approx 18$ μm at different scales.

2.2. Experimental Method. A photograph of the experimental setup is shown in Figure 2. The experimental setup includes an imaging system, glass experimental test cell, horizontal precision platform, droplet driving device, and light-emitting diode light source. The glass experimental test cell is assembled by a quartz glass square cylinder, fixed bracket, and 304 SS fiber. The droplet driving device is equipped with a precision mobile platform with 0.01 mm resolution and a more hydrophobic fiber, specifically a small poly-(tetrafluoroethylene) (PTFE) rod with a tapered tip. The tip of the PTFE rod was controlled to be within 100 μm.

The water droplets were first manually placed on the fiber under oil via a microsyringe, then one of the water droplets was slowly approached toward the other with the aid of a precision mobile platform with a hydrophobic PTFE rod. Coalescence events were observed from a side view using a high-speed camera (i-Speed 3, Olympus Corporation, Tokyo, Japan) equipped with a macro focus zoom lens, the images were

https://doi.org/10.1021/acsomega.3c01209
ACS Omega 2023, 8, 18019−18028

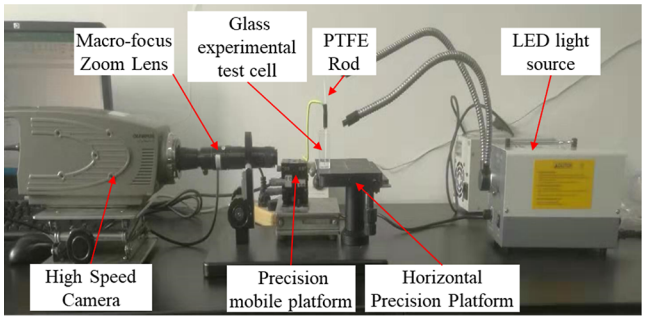

(a)

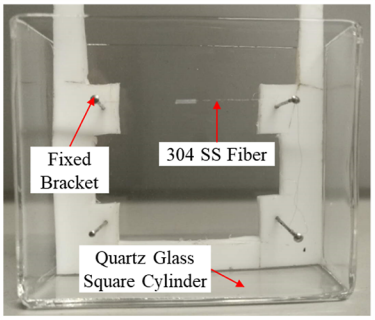

(b)

Figure 2. Photographs of the experimental setup. (a) Photograph of the assembled experimental setup. (b) Glass experimental test cell.

captured at an exposure time of 1/5000 s and recorded at 2000−5000 frames per second. To reduce the influence of the PTFE rod on the coalescence process of water droplets on fibers, when two water droplets are about to touch, the moving speed of the droplet should be as small as possible, so that the two water droplets touch gently, triggering the merging of the droplets. Images were processed by Image-Pro Plus software to obtain information, including the droplet size, morphology evolution, and so on. The size of the droplets was obtained by setting a reference object of known size. The time of one frame before the liquid bridge starts to expand is set to zero. All experiments were conducted at room temperature.

2.3. Presentation of Physical Parameters. To evaluate the relative importance of different forces on the droplet coalescence and self-removal behaviors on the fibers in oil, the following dimensionless physical parameters were adopted:

The Ohnesorge number, *Oh*, denotes the relative importance of the internal viscosity dissipation effect versus the surface tension energy effect.[44]

$$Oh = \mu_w / \sqrt{\rho_w \gamma_{ow} R_i} \quad (1)$$

where μ_w and ρ_w are the viscosity and density of water droplets, respectively, γ_{ow} is the oil−water interfacial tension, and R_i is the droplet radius.

The negative buoyancy of water droplets in oil can be calculated as follows

$$F_b = \frac{4}{3}\pi g R_i^3 (\rho_o - \rho_w) \quad (2)$$

and the settling velocity of a water droplet in oil can be estimated according to the Stokes formula

$$V = \frac{2}{9}\frac{\rho_w - \rho_o}{\mu_o} g R_i \quad (3)$$

where ρ_o and μ_o are the density and viscosity of the bulk fluid, respectively, and g is the gravitational constant. The settling velocity of merged droplets calculated here does not take into account the adhesion energy between droplets and fibers and the initial jumping velocity.

In this work, the droplet radius studied here ranged from 0.4 to 0.75 mm, according to the physical properties of the bulk fluids listed in Table 1, the corresponding Ohnesorge number (Oh), negative buoyancy (F_b), and settling velocity (V) can be calculated and the results were presented in Table 2.

Table 2. Corresponding Ohnesorge Number (Oh), Negative Buoyancy (F_b), and Settling Velocity (V) of Water Droplets Studied Here

bulk fluid	R_i/mm	Oh	$F_b \times 10^{-12}$/N	V/mm/s
n-C_6H_{14}	0.44	0.005	−1.202	0.227
	0.57	0.005	−2.614	0.381
	0.71	0.004	−5.052	0.591
n-$C_{12}H_{26}$	0.44	0.011	−0.898	0.079
	0.57	0.009	−1.953	0.132
	0.71	0.008	−3.774	0.205
C_7H_8	0.44	0.005	−0.472	0.101
	0.57	0.004	−1.026	0.170
	0.71	0.004	−1.982	0.264

As shown in Table 2, the number of Oh was varied only by a factor of 2 and the drop diameter was also varied by a factor of 2. According to the Ohnesorge number calculation formula, this number can be adjusted by changing the droplet radius or interfacial tension. However, in our experiments, it was difficult to achieve large-scale control of droplet radius or interfacial tension on fibers due to practical limitations. Coalescence was challenging to achieve with too low interfacial tension or too small droplets. Furthermore, in real oil−water emulsions, droplet sizes are usually larger than 10 μm, which implies that the Ohnesorge number values are within the range studied in our research. Therefore, we believe that our experiments provide useful insights into this phenomenon and reveal the governing mechanism of this phenomenon.

3. RESULTS AND DISCUSSION

3.1. Morphology Evolution of Water Droplet Coalescence on Hydrophobic Fibers in Oil. In this section, the effects of bulk fluid viscosity and oil−water interfacial tension on the coalescence behavior of droplet coalescence on hydrophobic fibers in oil were investigated.

3.1.1. Effect of Bulk Fluid Viscosity. According to the physical characteristics of liquid in Table 1, the viscosity and oil−water interfacial tension of n-C_6H_{14} and n-$C_{12}H_{26}$ are about 0.6393 and 1.3746 mPa s and 50.51 and 50.1 mN/m, respectively. Although the difference in density between the two fluids is about 13%, the effect of bulk fluid density on the coalescence and self-removal behavior was small compared to viscosity. Hence, n-C_6H_{14} and n-$C_{12}H_{26}$ were chosen as bulk fluid to study the effect of the viscosity of bulk fluid on the coalescence behavior of water droplets on hydrophobic fibers in oil.

Time-lapse images of the coalescence of two water droplets about 1 mm in diameter on hydrophobic fibers in n-C_6H_{14} and n-$C_{12}H_{26}$ are shown in Figure 3.

Comparing Figure 3a with Figure 3b, it was found that in n-C_6H_{14} and n-$C_{12}H_{26}$, the time from the beginning of water

https://doi.org/10.1021/acsomega.3c01209
ACS Omega 2023, 8, 18019−18028

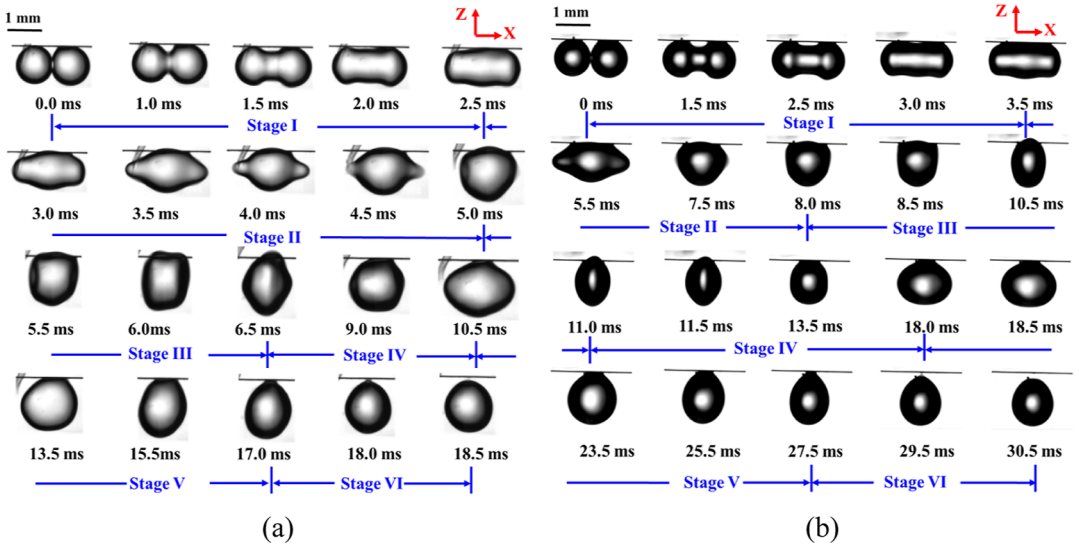

Figure 3. Effects of outer fluid viscosity on the morphology evolution of coalescence droplet on hydrophobic fibers. (a) Coalescence in n-C_6H_{14} and (b) coalescence in n-$C_{12}H_{26}$.

droplet coalescence to the detachment from the fibers is different, but the morphology evolution during the coalescence is similar. Generally, according to the morphology evolution of droplets along the X and Z axes, the process can be divided into six stages. First, the liquid bridge grows between the merging droplets. Second, the three-phase contact line retracts allowing the droplets to merge into a larger one. Third, the merged droplet's centroid descends rapidly along the Z-axis. Fourth, the merged droplet expands along the X-axis. Fifth, the centroid of the merged droplet descends along the Z-axis once more. Finally, the merged droplet sheds from the fiber.

During the initial two stages, the primary changes in the merged droplets' shape were due to the growth of the liquid bridge and the retraction of the three-phase contact line. These alterations facilitated the combination of two small droplets into a larger one. In the third stage, the centroid of the merged droplet rapidly descended along the Z axis, while the merged droplet remained attached to the fiber surface. Subsequently, the merged droplets undergo oscillations along the X, Y, and Z axes in the following three stages, until they eventually detached from the fibers due to the combined effects of gravity and fluid resistance. The fluid drag force is instrumental in overcoming the adhesion force between the droplet and the fiber, while simultaneously preventing the droplets from reattaching to the fiber surface, thereby ensuring a smooth detachment of the droplets under the influence of gravity.

According to time-lapse images of water droplet coalescence in n-C_6H_{14} (as shown in Figure 3a), as two droplets contact together (0 ms), a tiny liquid bridge is formed and driven by the capillary pressure, the liquid bridge expands rapidly from zero to just equal to the diameter of the initial droplets (2.5 ms), at which point the three-phase contact line reaches the maximum. Then, the merged droplet starts to shrink along the X-axis due to the excess surface energy and at 5.0 ms, the two droplets merged into a larger one. After the merging process in stage III, the resulting droplet quickly descended along the Z-axis within a remarkably short time of 1.5 ms. It is worth noting that unlike the coalescence of water droplets on superhydrophobic plates in air,[27,36,45] the merged droplets, in this case, remained attached to the fiber surface. Additionally, they continued to oscillate along both the Z-axis and X-axis even after stage III. The droplets were only separated from the fibers after a duration of approximately 18.5 ms.

The main reason for this is that the viscosity of the bulk fluid studied here is much higher than that of air, which hinders the detachment of water droplets from fibers. According to the Stokes drag equation, the drag force of bulk fluid to a droplet, $F_{drag} = 6\pi\mu_o R_i u$, where F_{drag} is the drag force, μ_o is the viscosity of the bulk fluid, and u is the instantaneous droplet velocity during the detaching process, is proportional to the viscosity of the bulk fluid. Thus, for droplet coalescence in oil, most of the excess surface energy is needed to overcome the viscosity dissipation energy, and only a small part of the excess surface energy is converted to kinetic energy. In addition, the small contact area between the water droplets and the fibers is not conducive to converting the excess surface energy into kinetic energy. Therefore, the detaching behavior of water droplets in oil is more difficult than that in air. The detaching of the merged droplets from the fibers mainly depended on the shrinkage of merged droplets rather than on jumping, as shown in Figure 3a.

The time-lapse images in Figure 3b depicting water droplet coalescence in n-$C_{12}H_{26}$ appeared to be similar to those in Figure 3a for n-C_6H_{14}, except for the fact that the coalescence process took longer for each stage in n-$C_{12}H_{26}$ compared to n-C_6H_{14}. In the first three stages, the coalescence time for n-C_6H_{14} was approximately 6.5 ms, while for n-$C_{12}H_{26}$, it was around 11 ms, which is roughly 1.7 times longer than that of n-C_6H_{14}. Similarly, during the last three stages, the coalescence time for n-C_6H_{14} and n-$C_{12}H_{26}$ was about 12 and 19.5 ms, respectively. This means that the coalescence time for n-$C_{12}H_{26}$ was also approximately 1.6 times longer than that of n-C_6H_{14}. This is because n-$C_{12}H_{26}$ has a higher viscosity compared to n-C_6H_{14}. As a result, the impact of the bulk fluid on droplet coalescence is more significant in n-$C_{12}H_{26}$, making droplet deformation more challenging, and leading to a longer coalescence time in this fluid.

Despite the water droplets in n-C_6H_{14} having a lower negative buoyancy than those in n-$C_{12}H_{26}$, the difference between the two is only approximately 25.2%, as indicated in Table 2. Therefore, the influence of gravity-buoyancy on the

https://doi.org/10.1021/acsomega.3c01209
ACS Omega 2023, 8, 18019−18028

coalescence process is not significant compared to the impact of the bulk fluid viscosity.

Moreover, although the under-oil WCA of a water droplet on SS fibers in n-$C_{12}H_{26}$ is larger than that in n-C_6H_{14}, as shown in Table 1, the viscosity of n-$C_{12}H_{26}$ is higher than that of n-C_6H_{14}. This results in larger viscosity dissipation energy, which leads to less kinetic energy of the merged droplet. Therefore, the influence of under-oil WCA was not significant in this case.

Figure 4 shows the time and time ratio of each stage for water droplet coalescence in n-C_6H_{14} and n-$C_{12}H_{26}$. As can be

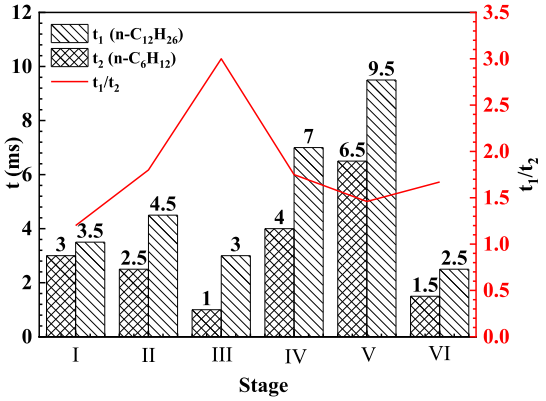

Figure 4. Time and time ratio of each stage for two droplets coalescing on hydrophobic fibers in n-C_6H_{14} and n-$C_{12}H_{26}$.

seen from this figure, the time of water droplet coalescence in the higher viscous bulk fluid (i.e., t_1), that is, in n-$C_{12}H_{26}$, is longer than that in n-C_6H_{14} (i.e., t_2), but the time ratio (t_1/t_2) is not a constant. The value of t_1/t_2 shows a tendency of first increasing and then decreasing during the coalescence process, and the maximum is reached at stage III, which is t_1/t_2 = 3.0.

Unlike the coalescence of water droplets in the air, in the viscous bulk fluids, the morphology evolution of merged droplets would be affected by the bulk fluid, especially those with larger viscosity. At stage I, the main morphology evolution was the liquid bridge expansion. The driving force for the liquid bridge expansion is the capillary pressure, $\Delta p \approx \gamma_{ow}R_i/r_c^2$, where r_c is the neck radius of the liquid bridge.[39] Because the radius of the liquid bridge at this stage is very small, the capillary pressure is so high that the influence of bulk fluids on the expansion of the liquid bridge can be ignored; thus, the difference between t_1 and t_2 was minimal. After this stage, however, the main morphology evolution was the deformation of merged droplets. The deformation rate was determined by excess surface energy and viscosity dissipation energy, which depended on the fluid properties of bulk fluid and droplets, as well as on the droplet's instantaneous velocity. Increasing the viscosity of bulk fluid or the instantaneous velocity of merged droplets both increase the viscosity dissipation energy, which will result in an increase in coalescence time. For droplet coalescence-induced self-removal on superhydrophobic surfaces, the maximum instantaneous velocity was reached at stage III.[25,46] Moreover, due to the higher viscosity of n-$C_{12}H_{26}$, the coalescence time at each stage was longer in n-$C_{12}H_{26}$ than in n-C_6H_{14} and this difference is especially evident at larger instantaneous velocity. Hence, the value of t_1/t_2 shows a tendency to increase and then decrease, reaching a maximum at stage III.

In summary, the viscosity of the bulk fluid significantly influences the morphology of merged droplets during the water droplet coalescence in oil. Higher viscosity results in longer coalescence times. And the impact of viscosity is more pronounced at higher instantaneous velocities of merged droplets. Hence, it is essential to have a thorough understanding of the bulk fluid's properties and the merging process dynamics to effectively control and optimize droplet coalescence behavior in oil.

3.1.2. Effect of Oil–Water Interfacial Tension. In this section, the influence of interfacial tension on the coalescence and detaching behavior of water droplets on hydrophobic fibers in n-C_6H_{14} and C_7H_8 was investigated, and the results are shown in Figure 5. The oil–water interfacial tension of n-

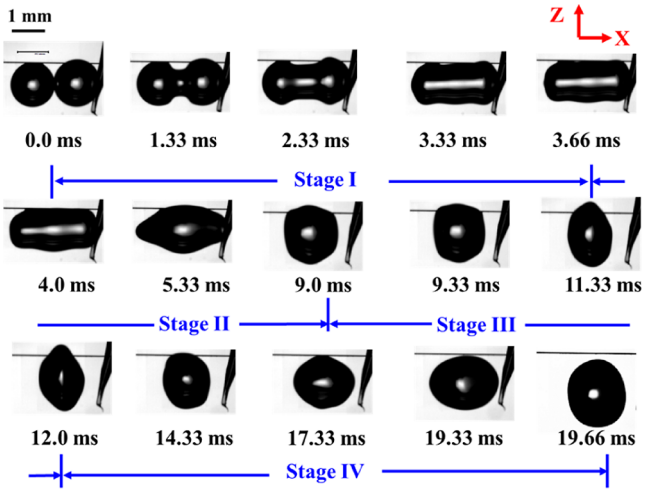

Figure 5. Morphology evolution of coalescence droplets on hydrophobic fibers in C_7H_8.

C_6H_{14} and C_7H_8 is 50.51 and 35.7 mN/m, respectively, as shown in Table 1. The diameter of the two water droplets studied here was also about 1.0 mm.

Comparing Figure 5 with Figure 3a, it can be found that in C_7H_8, the morphology evolution and the overall coalescence time of the merged droplets were similar to those in n-C_6H_{14}, but the number of coalescence stages was only four stages, and the coalescence time of each stage was longer than that in n-C_6H_{14}. It is well known that the driving force for the droplet morphology and droplet jumping is excess surface energy, which is proportional to the oil–water interfacial tension.[27,28] As shown in Table 1, the oil–water interfacial tension of C_7H_8 is 35.7 mN/m, which is only about 70.7% that of n-C_6H_{14}. Hence, the frequency of droplet morphology evolution in C_7H_8 was lower than that in n-C_6H_{14}, i.e., the time required for each stage of droplet deformation was larger than that in n-C_6H_{14}, as shown in Figure 6.

The coalescence time in C_7H_8 was similar to that in n-C_6H_{14}, despite fewer coalescence stages in C_7H_8, possibly due to a larger under-oil WCA on the 304 fibers in C_7H_8 than in n-C_6H_{14}. Table 1 shows that the under-oil WCA in n-C_6H_{14} and C_7H_8 is about 115.5 ± 2 and 120.25 ± 2°, respectively. Thus, under the influence of gravity, the merged droplet was more likely to detach from the fiber in C_7H_8 than in n-C_6H_{14} due to the larger contact angle. Despite the fact that the viscosity of C_7H_8 is lower than that of n-C_6H_{14}, the density of C_7H_8 is higher than that of n-C_6H_{14}. This means that the buoyancy of

https://doi.org/10.1021/acsomega.3c01209
ACS Omega 2023, 8, 18019−18028

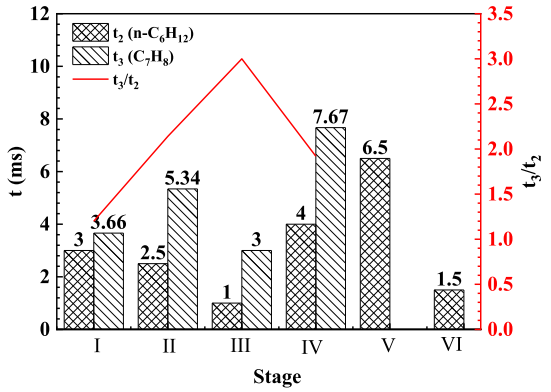

Figure 6. Time and time ratio of each stage for two droplets coalescing on superhydrophobic fibers in n-C_6H_{14} and C_7H_8.

water droplets in C_7H_8 is greater than that in n-C_6H_{14}, which could counterbalance the beneficial effect of lower viscosity.

Figure 6 presents the times and time ratios for each stage of two droplet coalescence in n-C_6H_{14} and C_7H_8. Even though the coalescence stage of water droplets in C_7H_8 occurred less rapidly than in n-C_6H_{14}, the coalescence time for each stage of water droplets in C_7H_8 (i.e., t_3) was longer than in n-C_6H_{14} (i.e., t_2). Interestingly, the ratio of t_3/t_2 exhibited the same trend as t_1/t_2 (as depicted in Figure 4), reaching a maximum during stage III. The reason for this is the same, as mentioned in Section 3.1.1, and is due to the influence of the viscosity of bulk fluid and the morphology evolution rate of merged droplets.

In summary, the coalescence and detaching of water droplets on hydrophobic surfaces in oils are influenced by various factors related to the bulk fluid. Lowering the viscosity of the bulk fluid promotes coalescence and self-removal of water droplets and reduces the coalescence time of each stage, while increasing the oil−water interfacial tension may lead to a higher frequency of droplet deformation. The total time for water droplet coalescence and detaching from hydrophobic fibers is determined by several factors, including the viscosity of the bulk fluid, the under-oil WCA, and the gravity-buoyancy effect. However, the effects of viscosity and under-oil WCA play a critical role in determining the coalescence time.

3.2. Expansion Dynamics of Liquid Bridge during the Coalescence Process. *3.2.1. Effect of Droplet Radius.* To better understand the influence of droplet radius on the coalescence behavior of water droplets in oil, the variations of the liquid bridge radius along the Z-axis with the coalescence time were studied. The average radius of the initial droplet, R_0, studied here varied from 0.44 to 0.71 mm, and the bulk fluid was n-$C_{12}H_{26}$, the results are shown in Figures 7 and 9.

As shown in Figure 7a, with the increase of coalescence time t, the expansion rate of the liquid bridge differed for different size droplets, but the curves for different droplet radii take on a similar character, i.e., varying trends are almost the same except the amplitudes are different. Moreover, the number of coalescence stages and the coalescence time for each stage are also the same for all droplets and are independent of the droplet size. The evolution of liquid bridges mainly exists from stage I to stage III. As the coalescence process enters stage IV (at 11 ms), all the curves show an oscillation with time t. For drop coalescence, capillary waves are generated as the droplet starts to merge and then travel along the droplet interface until reaching the droplet apex along the Z-axis, which results in the fluctuation of liquid bridge in the first three stages.[42] After the radius along the Z-axis reached the maximum, the merged droplet starts to retract at the beginning of stage IV. After that, merged droplets start to oscillate along the Z-axis and X-axis, respectively.

According to the capillary pressure equation, $\Delta p \approx \gamma_{ow} R_i / r_c^2$, the driving force for the liquid bridge expansion is proportional to the oil interfacial tension and droplet radius but scales inversely with the liquid bridge radius. Therefore, increasing the droplet radius, R_i, can accelerate the expansion of the liquid bridge, that is, larger droplets have a greater liquid bridge radius expansion rate.

In our experiment, we observed that the number of coalescence stages for water droplet coalescing on hydrophobic fibers in n-$C_{12}H_{26}$ was independent of the initial droplet radii, as shown in Figure 7a. However, according to Table 2, the settling velocity of a water droplet with a radius of 0.71 mm was approximately 2.6 times larger than that with a radius of 0.44 mm when the droplets were set in n-$C_{12}H_{26}$. If gravity had a significant effect on the coalescence and detachment process, it would be reflected in the time and stage of the coalescence. However, this was not observed. Therefore, it can be inferred that for water droplet coalescence on hydrophobic fibers in oils, the effect of gravity on the coalescence stage and time was not as significant as the effect of bulk fluid viscosity and

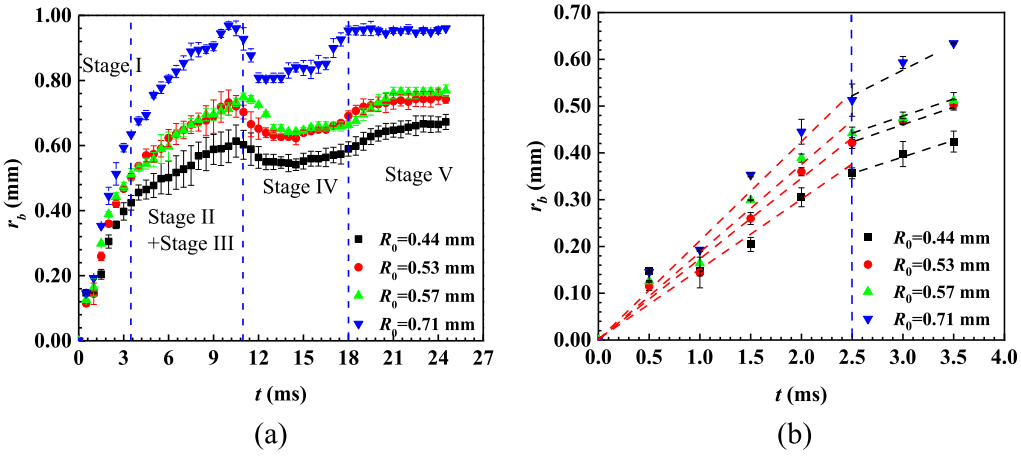

Figure 7. Variations of the liquid bridge radius (r_b) with the coalescence time (t) (a) throughout the whole process and (b) at stage I.

https://doi.org/10.1021/acsomega.3c01209
ACS Omega 2023, 8, 18019−18028

interfacial tension. As previously stated, in the detachment process of water droplets from hydrophobic fibers, the fluid drag force is crucial in preventing the droplets from reattaching to the fiber surface, thus ensuring a smooth detachment of the droplets under the influence of gravity, the detachment process was dominated by the bulk fluid viscosity.

For a better analysis, the liquid bridge radius at stage I is redrawn with the coalescence time, as illustrated in Figure 7b. It can be seen that the radius of the liquid bridge increases linearly with the coalescence time, and the overall growth of the liquid bridge is divided into two regions according to the transition of the slope of the line. The crossover time is about t = 2.5 ms. In the early stages of coalescence when $r_m \ll R_i$, the curvature of liquid bridge is very high and the gap width is very small, so the high-curvature meniscus can be represented by two straight lines with a distance of $2r_m$ apart. Meanwhile, the capillary pressure and the bridge expansion rate are also very high; thus, the effect of outer fluid on the liquid bridge can be ignored. The flow in the inner region of the liquid bridge provides the dominant contribution to the liquid expansion. Moreover, the time of liquid bridge expansion can be measured in units of $\mu_w R_i/\gamma_{ow}$. Therefore, the radius of liquid bridge at a certain time in the early stages of coalescence can be estimated on a fixed scale of $r_c \propto t\gamma_{ow}/\mu_w$,[39] that is, the liquid bridge expansion is linearly related to time.

The main reason for the transition of the slope of the line is the change in the azimuthal curvature of the liquid neck. According to the morphology evolution of coalescence water with coalescence time shown in Figure 3b, the liquid bridge can be classified into two types, i.e., the positive azimuthal curvature and the negative azimuthal curvature, based on the azimuthal curvature of the liquid neck. Hence, the variation of the liquid bridge at stage I can be further divided into two regions and named region I (positive azimuthal curvature) and region II (negative azimuthal curvature),[36] as shown in Figure 8. In region I, the two curvatures have opposite signs and can

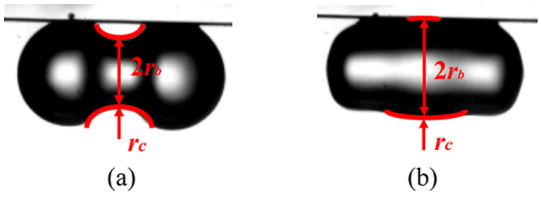

Figure 8. Two regions of droplet coalescence at stage I. (a) Region I (positive azimuthal curvature). (b) Region II (negative azimuthal curvature).

accelerate the expansion of the neck in opposite directions, but as the expansion goes on, the radius of curvatures increases, resulting in a gradual decrease in the driving force, so the expansion rate of the liquid bridge slows down. However, as the liquid bridge expands into region II, the azimuthal curvature of the neck bridge changes its direction, which now acts as a resistance to the expansion of the liquid bridge, so that the expansion rate of the liquid bridge slows down. That is also the reason why the curves in Figure 7a present a sharp increase followed by a gradual increase in the first three stages.

To better analyze the coalescence dynamics of water droplets in viscous bulk fluid, the liquid bridge radius was nondimensionalized by the average radius of the initial droplet, R_0, and the results are shown in Figure 9a,b. All the curves almost overlap at stage I, while there are some differences in the later stages, as illustrated in Figure 9a. For droplet coalescence and self-removal on hydrophobic fibers in oil, the coalescence dynamics were determined by the competition among capillary forces, viscous forces, inertial forces, and surface adhesion forces. At stage I, because the capillary forces and inertial forces are much larger than viscous forces and surface adhesion forces, the coalescence was dominated by capillary-inertial effects.[33] However, as the coalescence processes enter stage II, the effect of viscous forces increases and their influence is not negligible. So, the droplet morphology evolutions are determined by the competition among capillary forces, viscous forces, inertial forces, and surface adhesion forces, which accounts for the dependence of the curves in Figure 9a on the initial droplet radius, except for stage I.

In Figure 9b, the liquid radius at stage I is rescaled with R_0. It can be seen that all the data sets almost collapse into one line when plotted in a dimensionless form, and the radius of the liquid bridge expanding with time satisfies $r_b/R_0 \propto C_i t$, where C_i is a constant. For water droplet coalescence in n-$C_{12}H_{26}$, the constant $C_i \approx 0.321$. For droplet coalescence in viscous bulk fluid, the coalescence begins in the inertially limited viscous regime, that is, at the early stages, the dynamics are dominated by the inner fluid despite the much more viscous surroundings, and all the data are consistent with $r_b/R_0 \propto t$; at the later stage, there is competition between the inner and surrounding fluids, and the dynamics may be dominated by the inertial stress (given by the inner or outer fluid) or by the viscous stress in the outer fluid, which depends on the value of $\mu_o/\sqrt{\rho\gamma_{ow}R_0}$ (where ρ is the higher of the two-fluid densities).[33] In this study, the radius of water droplets R_i was less than 0.75 mm, and the corresponding dimensionless number $\mu_{out}/\sqrt{\rho\gamma_{ow}R_0} \sim O(10^{-3})$ was much lower than 0.3, so the dynamics at the later times were dominated by the inertial stress, which was given by the inner fluid.

As mentioned above, for the water droplet coalescence in n-$C_{12}H_{26}$, the expansion rate of the liquid bridge was affected by the droplet radius, increasing the droplet radius improved the expansion rate of the liquid bridge, but the dynamics of water droplet coalescence in oil were the same, that is, the drops began their coalescence in the inertially limited viscous regime and then transition to an inertia regime, which was given by the inner fluid at late times.

3.2.2. Effect of the Bulk Fluid. In this section, the effect of bulk fluid on the liquid bridge expansion was studied in n-C_6H_{14}, n-$C_{12}H_{26}$, and C_7H_8. The diameter of water droplets studied here was about 1.0 mm, and the results are shown in Figure 10.

As shown in Figure 10a, the radial expansion of the liquid bridge during coalescence in the three different bulk liquids showed similar characteristics. The curves first increase rapidly and then increase gradually, followed by oscillation with a certain amplitude. What differs between them is only the increase rate, amplitude, period, and the number of oscillations. All these indicate that the coalescence dynamics of water droplets were similar in n-C_6H_{14}, n-$C_{12}H_{26}$, and C_7H_8.

For a better observation, the curves of the first two stages were enlarged, as illustrated in Figure 10b. During the initial 2 ms, the curves are nearly indistinguishable from each other, but after this period, some variations emerge. Specifically, the expansion rate of the liquid bridge is the highest in n-C_6H_{14},

https://doi.org/10.1021/acsomega.3c01209
ACS Omega 2023, 8, 18019−18028

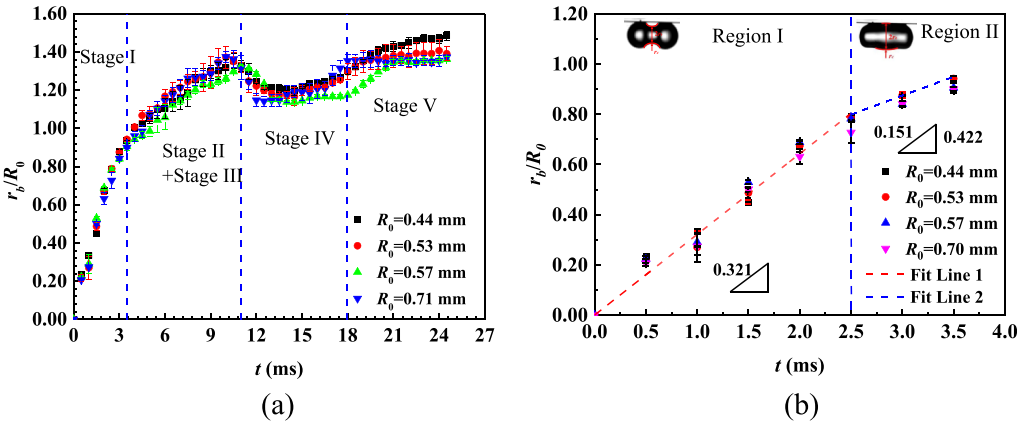

Figure 9. Variations of dimensionless liquid bridge radius with the coalescence time (a) throughout the whole process and (b) at stage I.

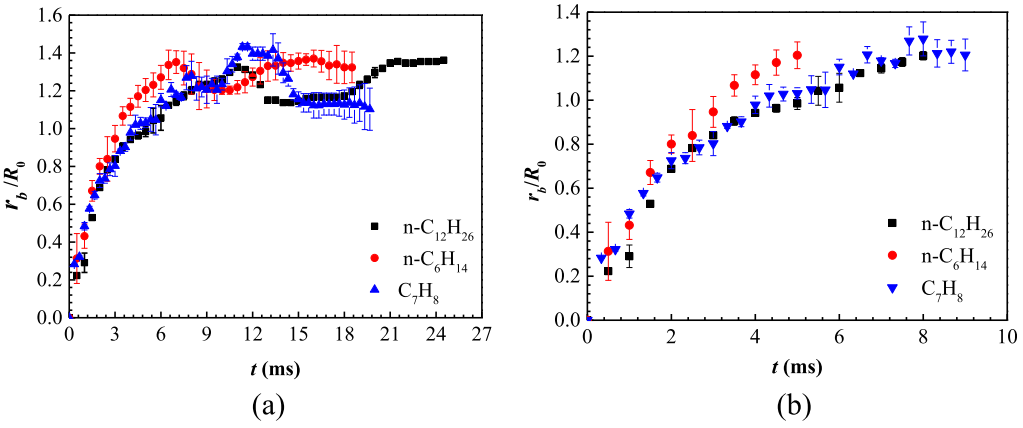

Figure 10. Effect of bulk fluid on the dimensionless liquid bridge radius (r_b/R_0) throughout whole process (a) and first two stages (b).

while the discrepancy in the liquid bridge expansion between C_7H_8 and n-$C_{12}H_{26}$ is not significant. For water droplet coalescence in oil, the influence of outer fluid on the liquid bridge expansion was not obvious due to the very high curvature of the early bridge, the dynamics were dominated by the inner fluid.[26] As the coalescence process progresses, the expansion of the liquid bridge slows down and the impact of the surrounding fluid on its expansion becomes more pronounced.

The viscosity and interfacial tension of the bulk fluids play a crucial role in the expansion of the liquid bridge. Higher interfacial tension will allow the liquid bridge to expand more quickly. While a higher viscosity surrounding the fluid will resist movement and deformation of the liquid bridge, making it harder for the bridge to expand. Table 1 reveals that among the three liquids, n-C_6H_{14} has intermediate viscosity but the highest interfacial tension. In contrast, n-$C_{12}H_{26}$ is similar to that of n-C_6H_{14}, but its viscosity is approximately 2 times higher than that of n-C_6H_{14}. C_7H_8 has the lowest viscosity, but its oil−water interfacial tension is also the lowest. Therefore, it is reasonable to observe the fastest expansion of liquid bridges in n-C_6H_{14}.

However, accounting for the influence of viscosity and interfacial tension on the dynamics of liquid bridge expansion is more challenging due to their complex nature and the possibility of competing mechanisms between them.[47] Further investigation is required to understand the detailed mechanisms involved.

From the preceding discussion, we can infer that the coalescence behavior of water droplets in oils exhibited similar dynamics. However, the extent to which the liquid bridge expands during coalescence was influenced by the interfacial tension and viscosity of the bulk fluid. While the impact of these factors on the bridge expansion was intricate, and there might be conflicting mechanisms at play, it is generally understood that higher interfacial tension and lower bulk fluid viscosity can both facilitate a bridge expansion.

4. CONCLUSIONS

This study investigated the impact of bulk fluid properties and droplet size on coalescence behaviors and dynamics of water droplets on hydrophobic fibers in oils. The morphology of merged droplets appeared similar during coalescence, but its evolution was significantly affected by bulk fluid properties. Lowering the bulk fluid viscosity promoted the coalescence and detachment of water droplets, resulting in a shorter coalescence time for each stage. Increasing the oil−water interfacial tension led to a higher frequency of droplet deformation and an increased number of coalescence stages.

The total time of water droplets on hydrophobic fibers in oils was dependent on several factors, including the viscosity of the bulk fluid, the under-oil WCA, and the gravity-buoyancy effect. While the viscosity and under-oil WCA had a more significant influence than the bulk fluid density.

The expansion dynamics of liquid bridge exhibited similar behavior for water droplet coalescence on hydrophobic fibers in oils. Larger droplets did accelerate the expansion of the

https://doi.org/10.1021/acsomega.3c01209
ACS Omega 2023, 8, 18019−18028

liquid bridge, but the coalescence time of droplets at each stage and the curves of the dimensionless liquid bridge radius (r_b/R_0) showed limited dependence on initial droplet radii. Moreover, the effects of bulk fluid viscosity and interfacial tension on the liquid bridge expansion were complex, but the impact of these factors was not significant at early coalescence stages. At the early stages, the droplets begin their coalescence in the inertially limited viscous regime and then transition to an inertia regime, which is given by the inner fluid at late times, and the liquid bridge radius expanding with time at early times satisfies $r_b/R_0 = C_i t$.

These findings contribute to a deeper understanding of the mechanism of water droplet coalescence and detachment on hydrophobic fibers in oil, which can be useful for many practical applications.

AUTHOR INFORMATION

Corresponding Author

Bingbing Li − *School of Energy and Chemical Engineering, Tianjin Renai College, Tianjin 301636, P. R. China;* orcid.org/0000-0002-2673-3179; Email: libb03@tju.edu.cn

Authors

Wei Tan − *School of Chemical Engineering and Technology, Tianjin University, Tianjin 300354, P. R. China*

Guiyu Liu − *School of Energy and Chemical Engineering, Tianjin Renai College, Tianjin 301636, P. R. China*

Mo Huang − *Audit Department, Jiangxi University of Chinese Medicine, Nanchang City, Jiangxi Province 330004, P. R. China*

Complete contact information is available at: https://pubs.acs.org/10.1021/acsomega.3c01209

Notes

The authors declare no competing financial interest.

ACKNOWLEDGMENTS

We acknowledge the funding support from Tianjin Research Innovation Project for Postgraduate Students (grant no. 2019KJ149).

REFERENCES

(1) Baena-Zambrana, S.; Repetto, S. L.; Lawson, C. P.; Lam, J. K. W. Behaviour of water in jet fuel—A literature review. *Prog. Aeronaut. Sci.* **2013**, *60*, 35−44.

(2) Kulkarni, P. S.; Patel, S. U.; Chase, G. G. Layered hydrophilic/hydrophobic fiber media for water-in-oil coalescence. *Sep. Purif. Technol.* **2012**, *85*, 157−164.

(3) Viswanadam, G.; Chase, G. G. Water−diesel secondary dispersion separation using superhydrophobic tubes of nanofibers. *Sep. Purif. Technol.* **2013**, *104*, 81−88.

(4) Li, B. B.; Xin, F.; Tan, W.; Zhu, G. R. Mesoscopic assessment of water droplet collision with a single stainless steel fiber in oil. *Desalin. Water Treat.* **2019**, *166*, 399−408.

(5) de Morais Coutinho, C.; Chiu, M. C.; Basso, R. C.; Ribeiro, A. P. B.; Gonçalves, L. A. G.; Viotto, L. A. State of art of the application of membrane technology to vegetable oils: A review. *Food Res. Int.* **2009**, *42*, 536−550.

(6) Li, B.; Qi, B.; Guo, Z.; Wang, D.; Jiao, T. Recent developments in the application of membrane separation technology and its challenges in oil-water separation: A review. *Chemosphere* **2023**, *327*, 138528.

(7) Mousa, H. M.; Fahmy, H. S.; Ali, G. A. M.; Abdelhamid, H. N.; Ateia, M. Membranes for Oil/Water Separation: A Review. *Adv. Mater. Interfac.* **2022**, *9*, 2200557.

(8) Sutrisna, P. D.; Kurnia, K. A.; Siagian, U. W. R.; Ismadji, S.; Wenten, I. G. Membrane fouling and fouling mitigation in oil−water separation: A review. *J. Environ. Chem. Eng.* **2022**, *10*, 107532.

(9) Zhao, X.; Cheng, L.; Jia, N.; Wang, R.; Liu, L.; Gao, C. Polyphenol-metal manipulated nanohybridization of CNT membranes with FeOOH nanorods for high-flux, antifouling and self-cleaning oil/water separation. *J. Membr. Sci.* **2020**, *600*, 117857.

(10) Liu, C.; Zhao, M.; Zheng, Y.; Cheng, L.; Zhang, J.; Tee, C. Coalescence-Induced Droplet Jumping. *Langmuir* **2021**, *37*, 983−1000.

(11) Wang, S.-W.; Peng, L.; Chen, J.-W.; Li, L. A comparative study of the self-propelled jumping capabilities of coalesced droplets on RTV surfaces and superhydrophobic surfaces. *Chin. Phys. B* **2021**, *30*, 046501.

(12) Chavez, R. L.; Liu, F.; Feng, J. J.; Chen, C. H. Capillary-inertial colloidal catapults upon drop coalescence. *Appl. Phys. Lett.* **2016**, *109*, 011601.

(13) Wisdom, K. M.; Watson, J. A.; Qu, X.; Liu, F.; Watson, G. S.; Chen, C. H. Self-cleaning of superhydrophobic surfaces by self-propelled jumping condensate. *Proc. Natl. Acad. Sci. U. S. A.* **2013**, *110*, 7992−7997.

(14) Feng, C.; Zhang, Z.; Li, J.; Qu, Y.; Xing, D.; Gao, X.; Zhang, Z.; Wen, Y.; Ma, Y.; Ye, J.; et al. A Bioinspired, Highly Transparent Surface with Dry-Style Antifogging, Antifrosting, Antifouling, and Moisture Self-Cleaning Properties. *Macromol. Rapid Commun.* **2019**, *40*, 1800708.

(15) Geyer, F.; D'Acunzi, M.; Sharifi-Aghili, A.; Saal, A.; Gao, N.; Kaltbeitzel, A.; Sloot, T. F.; Berger, R.; Butt, H. J.; Vollmer, D. When and how self-cleaning of superhydrophobic surfaces works. *Sci. Adv.* **2020**, *6*, No. eaaw9727.

(16) Li, T. Coalescence-Induced Jumping for Removing the Deposited Heterogeneous Droplets: A Molecular Dynamics Simulation Study. *J. Phys. Chem. B* **2022**, *126*, 8030−8038.

(17) Yan, X.; Ji, B.; Feng, L.; Wang, X.; Yang, D.; Rabbi, K. F.; Peng, Q.; Hoque, M. J.; Jin, P.; Bello, E.; et al. Particulate-Droplet Coalescence and Self-Transport on Superhydrophobic Surfaces. *ACS Nano* **2022**, *16*, 12910−12921.

(18) Liu, C.; Zhao, M.; Zheng, Y.; Lu, D.; Song, L. Enhancement and Guidance of Coalescence-Induced Jumping of Droplets on Superhydrophobic Surfaces with a U-Groove. *ACS Appl. Mater. Interfaces* **2021**, *13*, 32542−32554.

(19) Wang, K.; Ma, X.; Chen, F.; Lan, Z. Effect of a Superhydrophobic Surface Structure on Droplet Jumping Velocity. *Langmuir* **2021**, *37*, 1779−1787.

(20) Han, T.; Choi, Y.; Na, U.; Hwan Kim, M.; Jo, H. Fast nucleation of water by self-arrangement of hydrophilic crystals on a hierarchically structured surface promoting coalescence-induced droplet jumping. *Appl. Therm. Eng.* **2021**, *198*, 117444.

(21) Chen, X.; Wang, P.; Zhang, D.; Wu, J.; Ou, J. How surface orientation affects coalescence-induced droplet jumping behavior and subsequent atmospheric corrosion resistance of a superhydrophobic surface? *Corros. Sci.* **2022**, *197*, 110082.

(22) Li, C.; Liu, X.; Wang, P.; Zhang, D. Design of dual-scale composite structured superhydrophobic surfaces for atmospheric corrosion prevention based on coalescence-induced droplet jumping. *J. Taiwan Inst. Chem. Eng.* **2022**, *133*, 104308.

(23) Yu, Z.; Zhang, K.; Zhao, J.; Chen, S.; Lin, C.; Liu, Y. Coalescence-induced jumping of droplets on superhydrophobic substrates with a beam structure. *Appl. Surf. Sci.* **2022**, *582*, 152284.

(24) Li, Y.; Du, J.; Wu, X.; Lu, G.; Min, Q. How macrostructures enhance droplet coalescence jumping: A mechanism study. *Colloids Surf. A Physicochem. Eng. Asp.* **2023**, *658*, 130740.

(25) Feng, S.; Delannoy, J.; Malod, A.; Zheng, H.; Quere, D.; Wang, Z. Tip-induced flipping of droplets on Janus pillars: From local reconfiguration to global transport. *Sci. Adv.* **2020**, *6*, No. eabb4540.

(26) Gao, S.; Yuan, Z.; Wu, X. Coalescence-induced jumping of in-plane moving droplets: Effects of initial velocity and sideslip angle. *Chem. Eng. Sci.* **2023**, *265*, 118247.
(27) Li, B. B.; Xin, F.; Tan, W.; Zhu, G. R. A New Theoretical Model for Coalescence-Induced Droplet Jumping on Hydrophobic Fibers. *Ind. Eng. Chem. Res.* **2018**, *57*, 8299−8307.
(28) Li, B. B.; Xin, F.; Zhu, G. R.; Tan, W. Asymmetric coalescence-induced droplet jumping on hydrophobic fibers. *Chem. Eng. Sci.* **2019**, *201*, 298−308.
(29) Bazesefidpar, K.; Brandt, L.; Tammisola, O. Numerical simulation of the coalescence-induced polymeric droplet jumping on superhydrophobic surfaces. *J. Non-Newtonian Fluid Mech.* **2022**, *307*, 104872.
(30) Wen, R.; Lan, Z.; Peng, B.; Xu, W.; Yang, R.; Ma, X. Wetting Transition of Condensed Droplets on Nanostructured Superhydrophobic Surfaces: Coordination of Surface Properties and Condensing Conditions. *ACS Appl. Mater. Interfaces* **2017**, *9*, 13770−13777.
(31) Farokhirad, S.; Morris, J. F.; Lee, T. Coalescence-induced jumping of droplet: Inertia and viscosity effects. *Phys. Fluids* **2015**, *27*, 102102.
(32) Wang, H.; Lu, H.; Zhao, W. A review of droplet bouncing behaviors on superhydrophobic surfaces: Theory, methods, and applications. *Phys. Fluids* **2023**, *35*, 021301.
(33) Paulsen, J. D.; Carmigniani, R.; Kannan, A.; Burton, J. C.; Nagel, S. R. Coalescence of bubbles and drops in an outer fluid. *Nat. Commun.* **2014**, *5*, 3182.
(34) Sprittles, J. E.; Shikhmurzaev, Y. D. Dynamics of liquid drops coalescing in the inertial regime. *Phys. Rev. E: Stat., Nonlinear, Soft Matter Phys.* **2014**, *89*, 063008.
(35) Yokota, M.; Okumura, K. Dimensional crossover in the coalescence dynamics of viscous drops confined in between two plates. *Proc. Natl. Acad. Sci. U.S.A.* **2011**, *108*, 6395−6398.
(36) Wang, K.; Liang, Q.; Jiang, R.; Zheng, Y.; Lan, Z.; Ma, X. Morphology evolution and dynamics of droplet coalescence on superhydrophobic surfaces. *AIChE J.* **2018**, *64*, 2913−2921.
(37) Paulsen, J. D.; Burton, J. C.; Nagel, S. R.; Appathurai, S.; Harris, M. T.; Basaran, O. A. The inexorable resistance of inertia determines the initial regime of drop coalescence. *Proc. Natl. Acad. Sci. U. S. A.* **2012**, *109*, 6857−6861.
(38) Hopper, R. W. Coalescence of Two Equal Cylinders: Exact Results for Creeping Viscous Plane Flow Driven by Capillarity. *J. Am. Ceram. Soc.* **1984**, *67*, C-262−C-264.
(39) Eggers, J.; Lister, J. R.; Stone, H. A. Coalescence of liquid drops. *J. Fluid Mech.* **1999**, *401*, 293−310.
(40) Yao, W.; Maris, H. J.; Pennington, P.; Seidel, G. M. Coalescence of viscous liquid drops. *Phys. Rev. E: Stat., Nonlinear, Soft Matter Phys.* **2005**, *71*, 016309.
(41) Case, S. C.; Nagel, S. R. Coalescence in low-viscosity liquids. *Phys. Rev. Lett.* **2008**, *100*, 084503.
(42) Thoroddsen, S. T.; Takehara, K.; Etoh, T. G. The coalescence speed of a pendent and a sessile drop. *J. Fluid Mech.* **2005**, *527*, 85−114.
(43) Menchaca-Rocha, A.; Martinez-Davalos, A.; Nunez, R.; Popinet, S.; Zaleski, S. Coalescence of liquid drops by surface tension. *Phys. Rev. E: Stat., Nonlinear, Soft Matter Phys.* **2001**, *63*, 046309.
(44) Cheng, Y.; Xu, J.; Sui, Y. Numerical investigation of coalescence-induced droplet jumping on superhydrophobic surfaces for efficient dropwise condensation heat transfer. *Int. J. Heat Mass Transfer* **2016**, *95*, 506−516.
(45) Zhang, K.; Liu, F.; Williams, A. J.; Qu, X.; Feng, J. J.; Chen, C. H. Self-Propelled Droplet Removal from Hydrophobic Fiber-Based Coalescers. *Phys. Rev. Lett.* **2015**, *115*, 074502.
(46) Liu, F.; Ghigliotti, G.; Feng, J. J.; Chen, C.-H. Numerical simulations of self-propelled jumping upon drop coalescence on non-wetting surfaces. *J. Fluid Mech.* **2014**, *752*, 39−65.
(47) Montanero, J. M.; Ponce-Torres, A. Review on the Dynamics of Isothermal Liquid Bridges. *Appl. Mech. Rev.* **2020**, *72*, 01080.

https://doi.org/10.1021/acsomega.3c01209
ACS Omega 2023, 8, 18019−18028